Revista Brasileira de Geografia Física

ISSN:1984-2295

Homepage:https://periodicos.ufpe.br/revistas/rbgfe

Mapping the concentration of sea ice in the central Antarctic Peninsula with Sentinel 1 data

Fernando Luis Hillebrand[1], Ulisses Franz Bremer[2], Jorge Arigony-Neto[3], Cristiano Niederauer da Rosa[4], Cláudio Wilson Mendes Júnior[5], Juliana Costi[6], Marcos Wellausen Dias de Freitas[7]

[1]Doutorando do Programa de Pós-Graduação em Sensoriamento Remoto, Universidade Federal do Rio Grande do Sul (UFRGS) (fernando.hillebrand@rolante.ifrs.edu.br). [2]Doutor em Agronomia e Professor Adjunto do Programa de Pós-Graduação em Sensoriamento Remoto, Universidade Federal do Rio Grande do Sul (UFRGS) (bremer@ufrgs.br). [3]Doutor em Geografia Física e Professor Associado do Instituto de Oceanografia da Universidade Federal do Rio Grande (FURG) (jorgearigony@furg.br). [4]Doutorando do Programa de Pós-Graduação em Sensoriamento Remoto, Universidade Federal do Rio Grande do Sul (UFRGS) (cristianonrd@gmail.com). [5]Doutor em Geociências e Professor Adjunto do Programa de Pós-Graduação em Sensoriamento Remoto, Universidade Federal do Rio Grande do Sul (UFRGS) (claudio.mendes@ufrgs.br). [6]Pós-Doutoranda do Programa de Pós-Graduação em Modelagem Computacional, Universidade Federal do Rio Grande (FURG) (juliana.costi@furg.br). [7]Doutor em Sensoriamento Remoto e Professor Adjunto do Instituto de Geociências, Universidade Federal do Rio Grande do Sul (UFRGS) (mfreitas@ufrgs.br).

Artigo submetido em 22/03/2020 e aceito em 31/05/2020

A B S T R A C T

Sea ice acts as a thermal insulator between the ocean and the atmosphere and without it, the ocean will be free to emit heat to the atmosphere, influencing the formation of water bodies and ocean circulation. This article proposes the classification and identification of sea ice by means of Synthetic Aperture Radar (SAR) images in the C band, obtained by the Sentinel 1B satellite, Extra Wide Swath (EW) imaging mode under HH + HV polarizations, radiometrically calibrated and normalized to incidence angle at 30°. The study area covered the central oceanic region of the Antarctic Peninsula during the winter and early austral spring of 2018. Obtaining samples for the classification of SAR scenes was obtained through visual analysis of the target texture in Sentinel 2 optical images (Multispectral Instrument), false-color RGB compositions of the HH and HV polarizations (R-HH, G-HV, B-HV/HH and R-HH, G-HH, B-HV) and unsupervised classification through cluster analysis. Backscatter coefficients (σ°) were identified in the HH polarization of -8.0 to -12.6 dB for young ice and/or first-year ice, -2.1 to -7.3 dB for multiyear ice, and for the HV polarization of -19.3 to -24.2 dB for young ice and/or first-year ice and -6.8 to -13.4 dB for multiyear ice, making it possible to map the concentration of sea ice in the region of study by using these thresholds.
Keywords: backscatter coefficient, synthetic aperture radar, sea ice classification.

Mapeamento da concentração do gelo marinho na região central da Península Antártica com dados Sentinel 1

R E S U M O

O gelo marinho atua como isolante térmico entre o oceano e a atmosfera. Sem este, o oceano estará livre para emitir calor à atmosfera, influenciando a formação de massas d'água e circulação oceânica. Este artigo propõe a classificação e identificação do gelo marinho por meio de imagens *Synthetic Aperture Radar* (SAR) na banda C, obtidas pelo satélite Sentinel 1B, modo de imageamento *Extra Wide Swath* (EW), sob polarizações HH + HV, radiometricamente calibradas e normalizadas ao ângulo de incidência a 30°. A área de estudo abrangeu a região oceânica central da Península Antártica durante o inverno e início da primavera austral de 2018. A obtenção das amostras para a classificação das cenas SAR foi efetuada através da análise visual da textura dos alvos em imagens ópticas do Sentinel 2 (*Multispectral Instrument*), composições RGB falsa-cor das polarizações HH e HV (R-HH, G-HV, B-HV/HH e R-HH, G-HH, B-HV) e classificação não supervisionada por meio da análise de *cluster*. Foram identificados coeficientes de retroespalhamento (σ°) na polarização HH de -8,0 a -12,6 dB para gelo jovem e/ou gelo de primeiro ano, -2,1 a -7,3 dB ao gelo plurianual, e para a

polarização HV de -19,3 a -24,2 dB para gelo jovem e/ou gelo de primeiro ano e -6,8 a -13,4 dB ao gelo plurianual, possibilitando o mapeamento da concentração do gelo marinho na região de estudo pelo uso desses limiares.
Palavras-chave: coeficiente de retroespalhamento, radar de abertura sintética, classificação do gelo marinho.

Introduction

Sea ice has the potential to influence Earth's climate, as it allows the restriction of exchanges of heat, mass, momentum and chemical components between the ocean and the atmosphere. It also considerably reduces the solar radiation absorbed by the Earth's surface, and affects ocean circulation through changes in thermohaline circulation (Simpkins et al, 2012; Killworth, 1983). Deser et al. (2000) pointed out that the reduction of sea ice and, consequently, of albedo in the Polar Regions, increases the amount of solar radiation absorbed by the oceans leading to an increase on warming. In addition, sea ice provides an environment for the development of algae that serve as a food source for juvenile phases of Krill (*Euphausia* sp.), Primary organism in the food chain (Schaafsma et al., 2017), serving as a food source for whales, seals, penguins, squids and fish (Nicol and Brierley, 2010).

In Antarctica, since the 1980s, there has been a predominantly positive trend in the Southern Annular Mode (SAM) index. This mode of atmospheric variability is related to a change in atmospheric mass and, therefore, in atmospheric pressure (Gong and Wang, 1998). In the Bellingshausen Sea and the western region of the Weddell Sea, significant negative correlations were found between the increase in ice extent and the positive polarity of the SAM (Pezza et al., 2012). In view of this, it is essential to continuously monitor the fluctuations of the sea ice cover, mainly in regionalized analyzes, since the atmosphere does not behave as a single entity, which does not allow explaining the variability of the extent and concentration of sea ice across the Southern Ocean. (Lefebvre and Goosse, 2008).

This work proposes the determination of the backscattering behavior of Sentinel 1B SAR images, EW imaging mode in the Horizontal Horizontal (HH) and Horizontal Vertical (HV) polarizations, to delimit the concentration of sea ice in the central oceanic region of the Antarctic Peninsula. Bellingshausen and Weddell seas in the winter and austral spring of 2018.

Material and Methods

Study Site

The survey was carried out in the central region of the Antarctic Peninsula (Figure 1), where a maritime climate dominated by the influence of the Bellingshausen Sea is observed in the west (Martin and Peel, 1978). This region is characterized by an uninterrupted mountain range, with altitudes between 1,400 and 2,000 m, located in the continental region of the Antarctic Peninsula, forming a distinct climate barrier (Schwerdtfeger, 1984). The climate barrier influences the distinctive behavior of sea ice formation in relation to other regions in the Antarctic Continent.

Jacobs et al. (1979) and Meredith et al. (2008) demonstrate that in the western region of the Antarctic Peninsula hydrography is strongly influenced by the balance of air-ocean energy, the availability of Circumpolar Deep Water (CDW) along the slope of the platform and the melting of sea ice. Antarctic Surface Water (AASW), a relatively cold and fresh water body, occupies the surface layer. This layer undergoes significant changes throughout the year, such as heat loss and sea ice formation during autumn and winter.

In addition, the region has a highly productive ecosystem that supports marine populations whose abundance and geographical distribution have been affected by changes in sea ice conditions and atmospheric warming (Moffat and Meredith, 2018; Montes-Hugo et al., 2009; Clarke et al ., 2006).

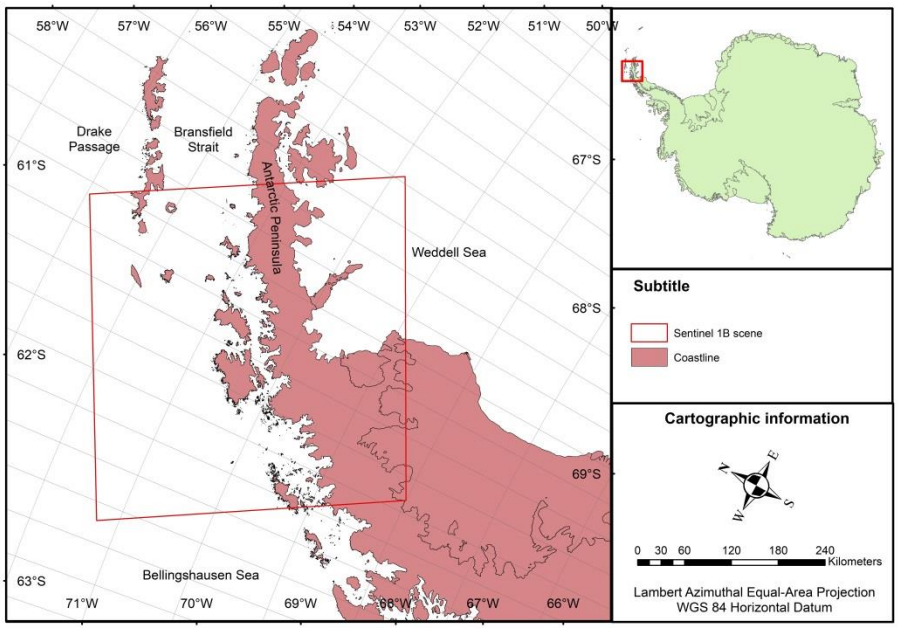

Figure 1. Study site location.

Sentinel 1 and 2 data

In this study, SAR images were used in the Sentinel 1B C band, in EW imaging mode, with HH + HV co-polarization and 25 m spatial resolution. Table 1 presents the data dates from the Sentinel 1B satellite used to elaborate the σ° thresholds of the SAR images, together with the different types of sea ice, and the Sentinel 2B optical images used to delimit the ice-covered regions.

The Sentinel 1 mission is composed of twin satellites 1A and 1B, being able to obtain SAR images in up to four imaging modes: Interferometric Wide swath (IW) with a 250 km bandwidth and 5 x 20 m resolution, Wave mode (WV) at 20 x 20 km and 5 x 5 m resolution, Strip Map (SM) at 80 km bandwidth and 5 x 5 m pixel resolution and EW with 400 km bandwidth and 20 x 40 pixel resolution m. In the products available there are also three processing levels including Level-0 (raw data), Level-1 (Single Look Complex data - SLC and Ground Range Detected - GRD) and Level-2 (Level-1 data with oceanographic information processing) (ESA, 2018). Sentinel 2 is a mission that provides multispectral images by means of an optical sensor with high spatial resolution, consisting of 13 spectral bands, three of which are visible and one of near infrared with a spatial resolution of 10 m, six infrared bands with 20 m three bands used for atmospheric correction of these images, with spatial resolution of 60 m.

With the σ° thresholds established, supervised classification and mapping of sea ice concentration was carried out on Sentinel 1B images with the same characteristics of direction, orbit number and imaging mode for the following dates: 01/05/2018, 05/13/2018, 08/17/2018, 08/29/2018, 09/10/2018 and 10/04/2018.

Table 1. Images from the Sentinel satellite located in the central region of the Antarctic Peninsula covering the Bellingshausen and Weddell Seas used to elaborate the σ° intervals of the SAR images next to the different types of sea ice.

Period	Date	Direction of orbit	Orbit	Sensor	Product type
September 2018	9/22/2018	Ascending	33	Sentinel 1B	S1B_EW_GRDH_1SDH
	9/25/2018	Descending	81	Sentinel 2B	S2B _MSIL1C
October 2018	10/28/2018	Ascending	33	Sentinel 1B	S1B_EW_GRDH_1SDH
	1/11/2018	Descending	38	Sentinel 2B	S2B _MSIL1C

Sea ice typology

An important aspect to be considered in the typological classification of sea ice using SAR images is the season. For this study, winter and austral spring images were considered, due to the minor alteration of first year ice backscatter and multi-annual ice, as melting sea ice affects the spectral response of the target. According to Barber (2005), the beginning of the melting of the multiyear ice is denoted by rapid drop in σ°, as the water contained in the snow, in its liquid state, absorbs energy in the microwave region (Figure 2). The first-year ice has its melting denoted by an increase in the active dispersion in the microwave region, melted snow grains with seawater in the basal part contribute to the dispersion of σ° in volume.

Regarding the number of sea ice types, Makynen and Hallikainen (2004) investigated in SAR images the classification of sea ice in up to eight typologies: open water leads, nilas, smooth level ice, rough level ice, slightly deformed ice, highly deformed ice, loose brah ice and frozen brash ice, all in bands C and X. They have found that it is possible to derive a classification table based on the mean and standard deviation values of σ° in a large number of SAR images, but its utility is compromised due to the intervals very close to the backscatter levels, with overlapping. Scheuchi et al. (2005) have successfully defined backscatter thresholds to identify the marine ice typology in each polarization (HH and HV), thus allowing discrimination between first year ice and multi-annual ice in ASAR Environmental Satellite (ENVISAT) images. Therefore, for this article, the sea ice typologies described by Comiso (2009) presented in table 2 were considered.

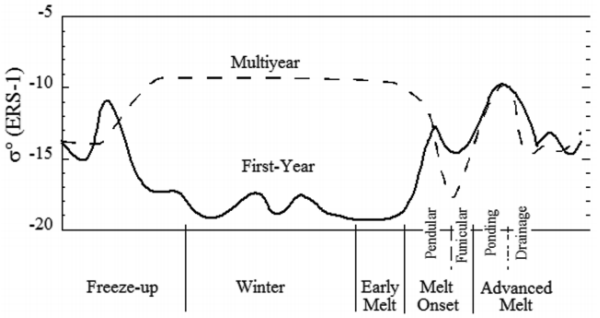

Figure 2. Seasonal evolution of σ° for first-year ice and multiyear ice during the annual sea ice cycle with SAR data in the C band of the European Remote Sensing satellite (ERS-1) in the Canadian Central Arctic. Source: Barber (2005).

Table 2. Typologies of sea ice based on the stages of ice development.

Development stage	Definition
Young ice and/or first-year ice	When the thin layer of sea ice reaches 15 to 30 cm in thickness, it becomes young ice. The young ice transition to first-year ice duration depends on the temperature, wind and location. In some stages, these two types are hardly distinguished, particularly when the ice layer is deformed and covered with snow.
Multiyear ice	Refers to the ice that lasted for at least two consecutive summers.

Source: Comiso (2009).

Processing Sentinel 1B Data

The processing of the Sentinel 1B images was performed in the Sentinel Application Platform (SNAP) software, following the flowchart illustrated in Figure 3. The first processing consisted of radiometric calibration, since the variations related to the antenna pattern affect the radiometric fidelity of a SAR imaging, causing radiometric distortions in the range direction, because the antenna transmits more power in the center of the beam than at its edges (Cunha, 2003). Thus, the process allows estimating the image noise by means of the power of the energy emitted by the pixels and removing the extreme values of the imaged target (Balss et al., 2010).

In sequence, the terrain correction of the SAR images was performed, as the topography has a significant influence on the geometric and radiometric properties of the images. Backscatter changes induced by relief must be treated as a systematic error and must be compensated (Loew and Mauser, 2007). For this step, the digital global elevation model Altimeter Corrected Elevations (ACE) was used, generated from the heights measured by the altimeter on board the ERS-1 with spatial resolution of 30 arc seconds.

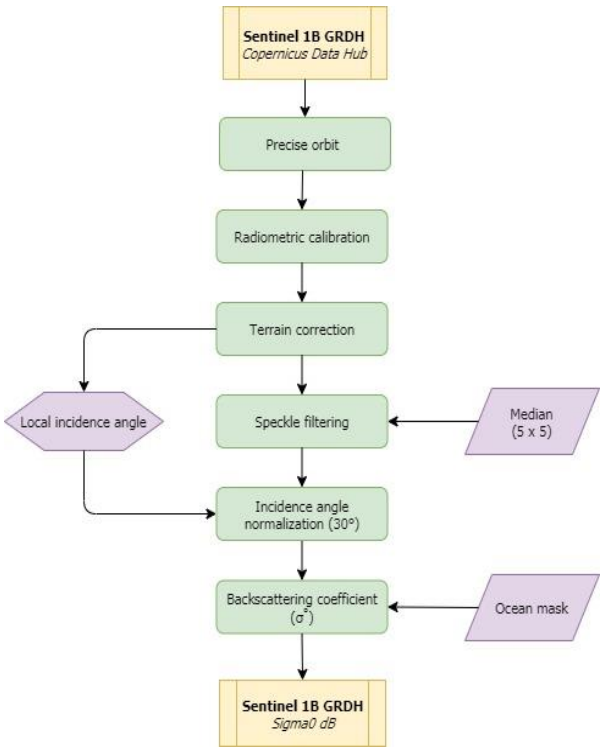

Figure 3. Processing steps for Sentinel 1B SAR images in the SNAP software.

To minimize the Speckle noise, we used processing with a median filter, with a movable window of 5 x 5 pixels. In addition to presenting high computational efficiency, it is one of the most efficient methods in the processing of SAR images for the classification of surface areas of snow and ice, preserving the abrupt changes of signal, without damaging the limits of the features in the images (Arigony-Neto, 2007).

The variation in σ° makes it difficult to define normalized backscatter bands for different targets therefore it is necessary to correct these variations within the different angles of incidence in the five sub-bands of SAR image imaging in EW mode. Mladenova et al. (2013) and Topouzelis (2016) proposed a method for cosineidal normalization of the backscattered signal, limiting the variations of σ° within the different angles of incidence (equation 1), also successfully applied by Zhou and Zheng (2017).

$$\sigma^0_{ref} = \frac{\sigma^0_\theta \cos^2(\theta_{ref})}{\cos^2(\theta)} \quad (1)$$

Where: σ^0_{ref}: Normalized backscatter coefficient; θ: Local incident angle; σ^0_θ: Backscatter coefficient measured; θ_{ref}: Angle of reference, being applied for this study 30°.

To perform the classification of SAR images, the digital pixel backscatter values were converted to decibels (dB).

Supervised classification of sea ice typology

Firstly, the regions covered with sea ice were delimited by means of optical images from the Sentinel 2 MultiSpectral Instrument (MSI) sensor (Red, Green, Blue - RGB 432) from 25/09/2018 and 11/01/2018. However, optical images do not allow to accurately allocating samples corresponding to the types of multiyear ice or young ice and/or first-year ice. For this, complementary analyzes obtained through the visual interpretation of these false-color compositions, combined with the unsupervised clustering classification (K-means) of the false-color colored compositions of the SAR images of Sentinel 1B (R-HH, G -HV, B-HV/HH and R-HH, G-HH, B-HV) from 09/22/2018 and 10/28/2018 (Figure 4).

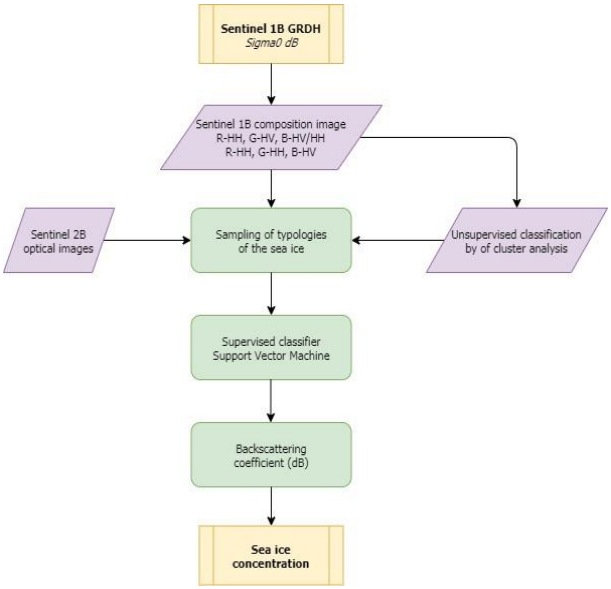

Figure 4. Supervised classification steps for mapping sea ice concentration.

False-color compositions are color images generated from three independent images in shades of gray, each one assigned to a given color channel (e.g, RGB color space).Makynen and Karvonen (2017) determined the concentration of sea ice through the discrimination between open water and sea ice, where the edge of the ice was extracted by different segmentation methods such as texture analysis, through local autocorrelation and backscattering of the ratio of HH/HV polarization. Thus, in the composition R-HH, G-HH, B-HV, it is possible to observe multiyear ice in white color and open water in dark color. In the composition R-HH, G-HV, B-HV/HH there is open water with bluish color, new ice with strongly reddish tones and

young ice and/or first-year ice with color varying between orange and gray, with its intensity depends on the surface roughness (Figure 5). Despite the color distinction of sea ice typologies, the establishment of backscatter intervals for new ice and open water in time series analysis has strong limitations.

The K-means unsupervised classification consists of grouping pixels using the minimum distance technique, to a number of classes defined by the user without the need for prior training of the classifier (Coleman and Andrews, 1979). Thus, the result of this process allowed the identification of some unique classes, but with a very small zonal extension and that could not be recognized in the visual interpretation of the false-color compositions.

From this set of information, representative sample polygons were extracted for each type of sea ice. These samples of the different types of sea ice (multiyear ice or young ice and/or first-year ice) were applied to the supervised classifier Support Vector Machine (SVM).

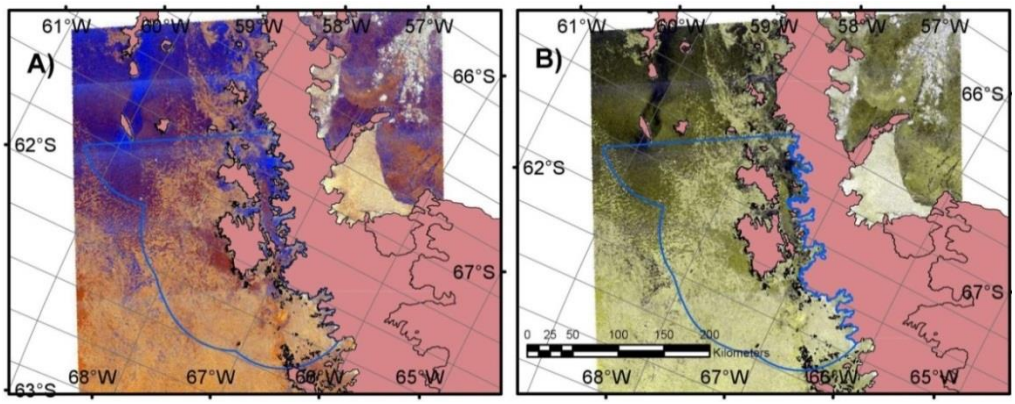

Figure 5. False-color composition of SAR images from Sentinel 1B, EW imaging mode, registered on 09/22/2018: A) RGB - HH, HV, HV/HH and B) RGB - HH, HH, HV.

Calculation of sea ice concentration

The calculation of the sea ice concentration was performed by superimposing a regular grid on the classified image that contained the delimitation of the regions covered with sea ice or open water. Through the predetermined grid size, zonal statistical tools can be applied using equation 2 (Karvonen, 2017) to calculate the ice concentration. The window size used for this article was 15 x 15 pixels, following studies by Zakhvatkina et al. (2013) and Gong et al. (2017), who concluded that this size would be more adequate in obtaining subsets for estimation of sea ice concentration through SAR data.

$$C_i = \frac{A_{ice}}{A_{tot}} = 1 - \frac{A_{ow}}{A_{tot}} \qquad (2)$$

Where: C_i: Ice concentration; A_{tot}: Total area; A_{ice}: Area of the fraction of young ice and/or first-year ice and multiyear ice within the total area; A_{ow}: Area of the open water fraction within the total area. The concentration of sea ice can be given as a pure ratio (range 0 to 1), 0 for open water or 1 for ice, as also expressed as a percentage (0% to 100%)

Results and Discussion

Backscatter thresholds (σ°) of Sentinel 1B images

In the classified images, the threshold values of backscattering for each target and polarization (HH + HV) were obtained, resulting in the following maximum and minimum values, at the 90% confidence level, according to table 3 and their respective means and standard deviations in table 4.

The low standard deviation found for supervised classifications is related to sampling carried out in the same period of the year, location of the SAR image (orbit and scene), imaging mode (EW) and the incidence angle normalized to 30°. Bovith and Andersen (2005) reported that the classification could be limited or restricted due to the interaction between the parameters of the SAR system and the surface properties, that is, geographic location and season of the year in which the image was recorded.

HV cross polarization backscattering has no sensitivity to the angle of incidence of the imaging and has less sensitivity to wind speed (Makynen and Hallikainen, 1998; Arkett et al.,

2003; Leshkevich and Nghiem, 2007; Partington et al., 2010). Thus, the separation of multiyear ice from first-year ice is satisfactory with the insertion of the cross polarization HV next to the simple polarization HH in band C.

The delimitation of the sea ice typology in the HH polarization by the SAR is improved including the HV cross polarization (Vachon and Wolfe, 2011). Particularly at angles below 35°, the cross-polarized channel may provide additional information about sea ice (Scheuchl et al., 2004). Partington et al. (2010) point out that open water, first-year ice and multiyear ice are efficiently discriminated, but other types of ice cannot be accurately identified by the HH/HV polarization ratio due to the high signal noise.

Table 3. Maximum and minimum values of σ° (dB) for the different types of sea ice.

Typology	September 2018				October 2018			
	HH		HV		HH		HV	
	σ° max	σ° min	σ° max	σ° min	σ° max	σ° min	σ° max	σ° min
Young ice and/or first-year ice	-7.9	-12.6	-19.1	-24.5	-8.1	-12.5	-19.4	-23.8
Multiyear ice	-1.9	-6.8	-6.6	-12.6	-2.2	-7.7	-7.0	-14.1

Table 4. Mean and standard deviation of σ° (dB) for different types of sea ice.

Typology	Mean				Standard deviation			
	HH		HV		HH		HV	
	σ° max	σ° min	σ° max	σ° min	σ° max	σ° min	σ° max	σ° min
Young ice and/or first-year ice	-8.0	-12.6	-19.3	-24.2	0.14	0.07	0.21	0.49
Multiyear ice	-2.1	-7.3	-6.8	-13.4	0.21	0.64	0.28	1.06

Mapping of sea ice concentration

The calculation of sea ice concentration by algorithms for SAR sensors with single polarization is restricted, since classification is limited by the interactions between the parameters of the Radio Detection and Ranging (RADAR) system, such as wavelength, polarization, angle incidence and surface properties (Bovith and Andersen, 2005). Figure 6 illustrates the mapping of the sea ice concentration in 2018 using Sentinel 1B co-polarized HH and HV images, EW imaging mode, with a normalized incidence angle of 30°. There is an expansion in the concentration of sea ice (young ice and/or first-year ice) over winter and early austral spring, with some coastal regions located in the Weddell Sea showing a constant concentration of 100% over the evaluated period, being predominated by multiyear ice, as identified in the false-color RGB compositions.

The temporal analysis of the sea ice concentration was restricted to the winter and austral spring of 2018, since Sentinel 1B SAR scenes were not available for this region of the Antarctic Peninsula in the Copernicus Data Hub database, with identical characteristics in the imaging mode and polarizations used in this study.

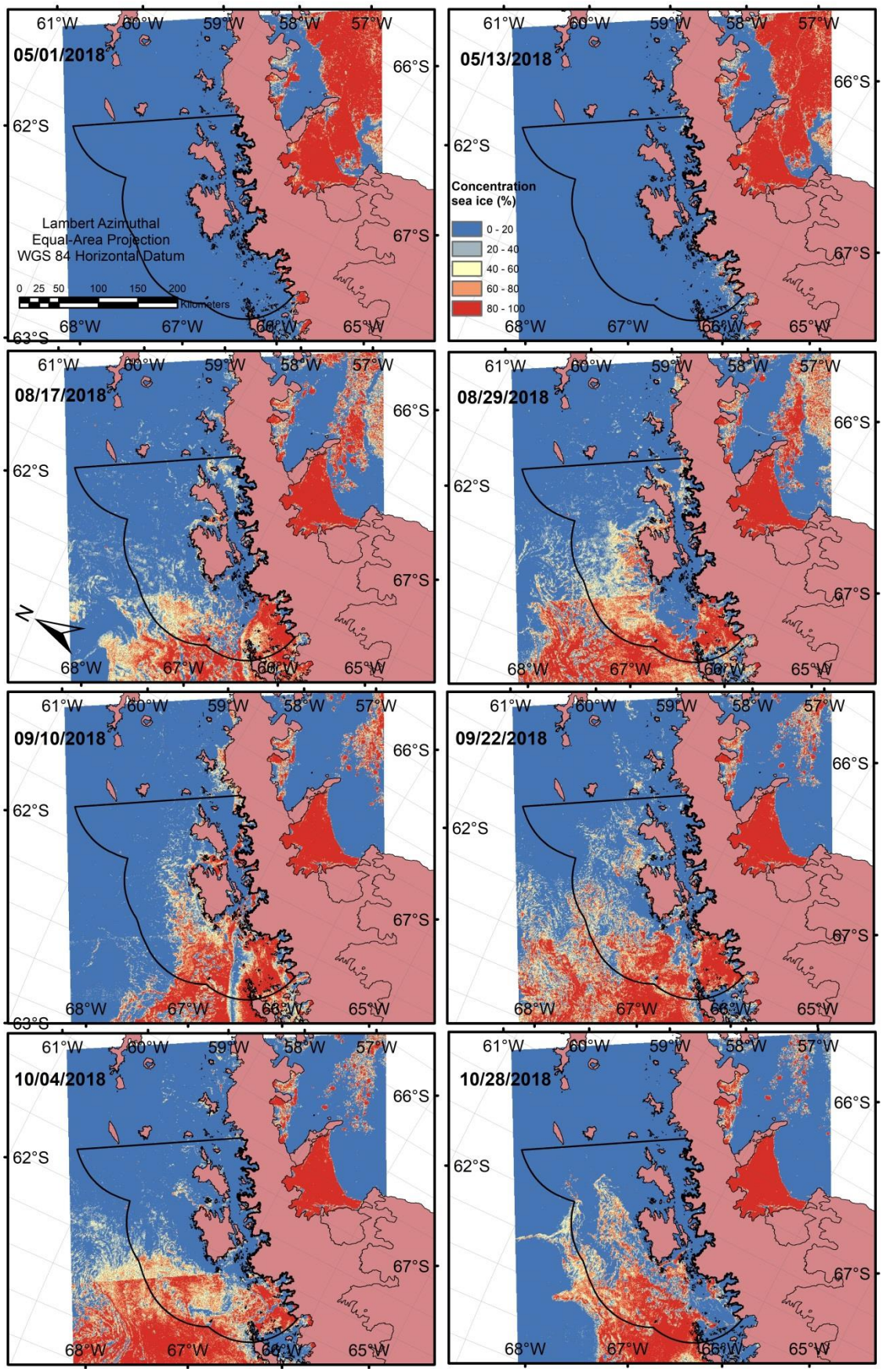

Figure 6. Concentration of sea ice obtained in Sentinel 1B SAR images under HH and HV co-polarization, EW imaging mode, with a normalized incidence angle of 30°.

Conclusions

From this study, the following backscatter coefficients were obtained for mapping sea ice: in polarization HH -8 to -12.6 dB for young ice and/or first-year ice, -2.1 to -7.3 dB to multiyear ice, and in the HV -19.3 to -24.2 dB polarization for young ice and/or first-year ice and -6.8 to -13.4 dB for multiyear ice. Thus, it is recommended to use these thresholds represented in σ° for studies in the typological analysis of sea ice in the central region of the Antarctic Peninsula covering the Bellingshausen and Weddell Seas, considering that the Sentinel 1B SAR images must be radiometrically calibrated and normalized to the incidence angle at 30°.

However, when using Sentinel 1B SAR images with double polarization (HH + HV) that consider broader typological classifications of sea ice for the backscattering analysis as presented in this study, it is necessary to consider the current weather conditions when interpreting the results on recording the images of the evaluated region. Given this, for other regions of the Southern Ocean, it is recommended to carry out analyzes of backscatter thresholds based on local data, and the methodology proposed in this study can be applied.

One of the advantages in the proposed methodology was to produce more accurate and detailed data of the concentration of sea ice in coastal regions from Sentinel 1 images, which have higher spatial resolution than the ones acquired from passive remote sensors, such as the Advanced Microwave Scanning Radiometer (AMSR) and the Special Sensor Microwave Imager/Sounder (SSMIS). Images from these last sensors have low spatial resolution ad have been used for the systematic mapping of ice concentration, record images with low spatial resolution and the mapping of sea ice concentration is carried out by means of algorithms that consider the brightness temperature of the targets.

Acknowledgements

The authors would like to thank the Instituto Federal de Educação, Ciência e Tecnologia do Rio Grande do Sul (IFRS) and the Coordenação de Aperfeiçoamento de Pessoal de Nível Superior - Brasil (CAPES) for promoting the development of this research.

References

Arigony-Neto, J.; Rau, F.; Saurer, H.; Jaña, R.; Simões, J.C.; Vogt, S. 2007. A time series of SAR data for monitoring changes in boundaries of glacier zones on the Antarctic Peninsula. Annals of Glaciology 46, 55-60.

Arkett, M.; Flett, D.; De Abreu, R. 2003. C-band multiple polarization SAR for ice monitoring– What can it do for the Canadian ice service. In: Proceedings of Envisat Symposium, Montreux, Switzerland, 23-27.

Balss, U.; Breit, H.; Fritz, T. 2010. Noise-related radiometric correction in the TerraSAR-X multimode SAR processor. IEEE Transactions on Geoscience and Remote Sensing 48, 741-750.

Barber, D.G. 2005. Microwave remote sensing, sea ice and Arctic climate. La Physique au Canada 61, 105-111.

Bovith, T; Andersen, S. 2005. Sea ice concentration from single-polarized SAR data using second-order grey level statistics and learning vector quantization. Danish Meteorological Institute: Scientific Report 05-04, 39 pp.

Clarke, A; Murphy, E.J.; Meredith, M.P.; King, J.C.; Peck, L.S.; Barnes, D.K.; Smith, R.C. 2006. Climate change and the marine ecosystem of the western Antarctic Peninsula. Philosophical Transactions of the Royal Society B: Biological Sciences 362 (1477), 149-166.

Coleman, H.B.; Andrews, H.C. 1979. Image segmentation by clustering. Proceedings of the IEEE 67, 773-785.

Comiso, J.C. 2009. Polar Oceans from Space. New York: Springer, 507 pp.

Cunha, E.R.S.P. 2003. Integração Digital de Imagens de Radar e Landsat-TM com dados Geológicos e Aerogamaespectrométricos no Auxílio ao Mapeamento Geológico da Região do Complexo Granítico Estrela, Pará. São José dos Campos: Dissertação de Mestrado, Instituto Nacional de Pesquisas Espaciais, 147 pp.

Deser, C.; Walsh, J.E.; Timlin, M.S. 2000. Arctic sea ice variability in the context of recent atmospheric circulation trends. Journal of Climate 13, 617-633.

Gong, C.; Zhang, W.; Zhang, S.; Fan, W.; Luo, L.; Hu, Y. 2017. Sea ice features extraction near the South Shetland Islands with Sentinel-1 SAR data. In: AOPC 2017: Optical Sensing and Imaging Technology and Applications. International Society for Optics and Photonics 10462T, 1-6.

Gong, D.; Wang S. 1998. Antarctic oscillation: concept and applications. Chinese Science Bulletin 43, 734-738.

Jacobs, S.S.; Gordon, A.L.; Amos, A.F. 1979. Effect of glacial ice melting on the Antarctic Surface Water. Nature 277, 469-471.

Karvonen, J. 2017. Baltic sea ice concentration estimation using sentinel-1 SAR and AMSR-2 microwave radiometer data. IEEE Transactions on Geoscience and Remote Sensing 55, 2871-2883.

Killworth, P.D. 1983. Deep convection in the world ocean. Reviews of Geophysics, 21 (1), 1-26.

Lefebvre, W.; Goosse, H. 2008. An analysis of the atmospheric processes driving the large-scale winter sea ice variability in the Southern Ocean. Journal of Geophysical Research: Oceans 113 (C2), 1-15.

Leshkevich, G.A.; Nghiem, S.V. 2007. Satellite SAR remote sensing of Great Lakes ice cover, part 2. Ice classification and mapping. Journal of Great Lakes Research 33, 736-750.

Loew, A.; Mauser, W. 2007. Generation of geometrically and radiometrically terrain corrected SAR image products. Remote Sensing of Environment 106, 337-349.

Makynen, M.; Hallikainen, M. 1998. C-band backscattering signatures of Baltic sea ice. In: IGARSS '98. Sensing and Managing the Environment. 1998 IEEE International Geoscience and Remote Sensing. Symposium Proceedings, 983-985.

Makynen, M.; Hallikainen, M. 2004. Investigation of C-and X-band backscattering signatures of Baltic Sea ice. International Journal of Remote Sensing 25, 2061-2086.

Makynen, M.; Karvonen, J. 2017. Incidence angle dependence of first-year sea ice backscattering coefficient in SENTINEL-1 SAR imagery over the Kara Sea. IEEE Transactions on Geoscience and Remote Sensing 55, 6170-6181.

Martin, P.J.; Peel, D.A. 1978. The spatial distribution of 10 m temperatures in the Antarctic Peninsula. Journal of Glaciology 20 (83), 311-317.

Meredith, M.P.; Brandon, M.A.; Wallace, M.I.; Clarke, A.; Leng, M.J.; Renfrew, I.A.; King, J.C. 2008. Variability in the freshwater balance of northern Marguerite Bay, Antarctic Peninsula: results from δ18O. Deep Sea Research Part II: Topical Studies in Oceanography 55, 309-322.

Mladenova, I.E.; Jackson, T.J.; Bindlish, R.; Hensley, S. 2013. Incidence angle normalization of radar backscatter data. IEEE Transactions on Geoscience and Remote Sensing 51, 1791-1804.

Moffat, C.; Meredith, M. 2018. Shelf-ocean exchange and hydrography west of the Antarctic Peninsula: a review. Philosophical Transactions of the Royal Society A: Mathematical, Physical and Engineering Sciences 376.

Montes-Hugo, M.; Doney, S.C.; Ducklow, H.W.; Fraser, W.; Martinson, D.; Stammerjohn, S.E.; Schofield, O. 2009. Recent changes in phytoplankton communities associated with rapid regional climate change along the western Antarctic Peninsula. Science 323 (5920), 1470-1473.

Nicol, S.; Brierley, A.S. 2010. Through a glass less darkly - new approaches for studying the distribution, abundance and biology of euphausiids. Deep Sea Research Part II: Topical Studies in Oceanography 57, 496-507.

Partington, K.C.; Flach, J.D.; Barber, D.; Isleifson, D.; Meadows, P.J.; Verlaan, P. 2010. Dual-polarization C-band radar observations of sea ice in the Amundsen Gulf. IEEE Transactions on Geoscience and Remote Sensing 48, 2685-2691.

Pezza, A. B.; Rashid, H. A.; Simmonds, I. 2012. Climate links and recent extremes in antarctic sea ice, high-latitude cyclones, Southern Annular Mode and ENSO. Climate Dynamics 38, 57-73.

Schaafsma, F.L.; Kohlbach, D.; David, C.; Lange, B.A.; Graeve, M.; Flores, H.; Van Franeker, J.A. 2017. Spatio-temporal variability in the winter diet of larval and juvenile Antarctic krill, Euphausia superba, in ice-covered waters. Marine Ecology Progress Series 580, 101-115.

Scheuchi, B.; Caves, R.; Flett, D.; De Abreu, R.; Arkett, M.; Cumming, I. 2005. The potential of cross-polarization information for operational sea ice monitoring. In: Envisat e ERS Symposium, 572.

Scheuchl, B.; Flett, D.; Caves, R.; Cumming, I. 2004. Potential of RADARSAT-2 data for operational sea ice monitoring. Canadian Journal of Remote Sensing 30, 448-461.

Schwerdtfeger, W. 1984. Weather and Climate of the Antarctic. Amsterdam: Elsevier, 261 pp.

Simpkins, G.R.; Ciasto, L.M.; Thompson, D.W.; England, M.H. 2012. Seasonal relationships between large-scale climate variability and Antarctic sea ice concentration. Journal of Climate 25, 5451-5469.

Topouzelis, K.; Singha, S.; Kitsiou, D. 2016. Incidence angle normalization of Wide Swath SAR data for oceanographic applications. Open Geosciences 8, 450-464.

Vachon, P.W.; Wolfe, J. 2011. C-band cross-polarization wind speed retrieval. IEEE Geoscience and Remote Sensing Letters 8, 456-459.

Zakhvatkina, N.Y.; Alexandrov, V.Y.; Johannessen, O.M.; Sandven, S.; Frolov, I.Y. 2013. Classification of sea ice types in ENVISAT synthetic aperture radar images. IEEE Transactions on Geoscience and Remote Sensing 51, 2587-2600.

Zhou, C.; Zheng, L. 2017. Mapping radar glacier zones and dry snow line in the Antarctic Peninsula using Sentinel-1 images. Remote Sensing 9, 1-19.